Volume 54 | Number 62 | 11 August 2018 | Pages 8537–8656

ChemComm

Chemical Communications

rsc.li/chemcomm

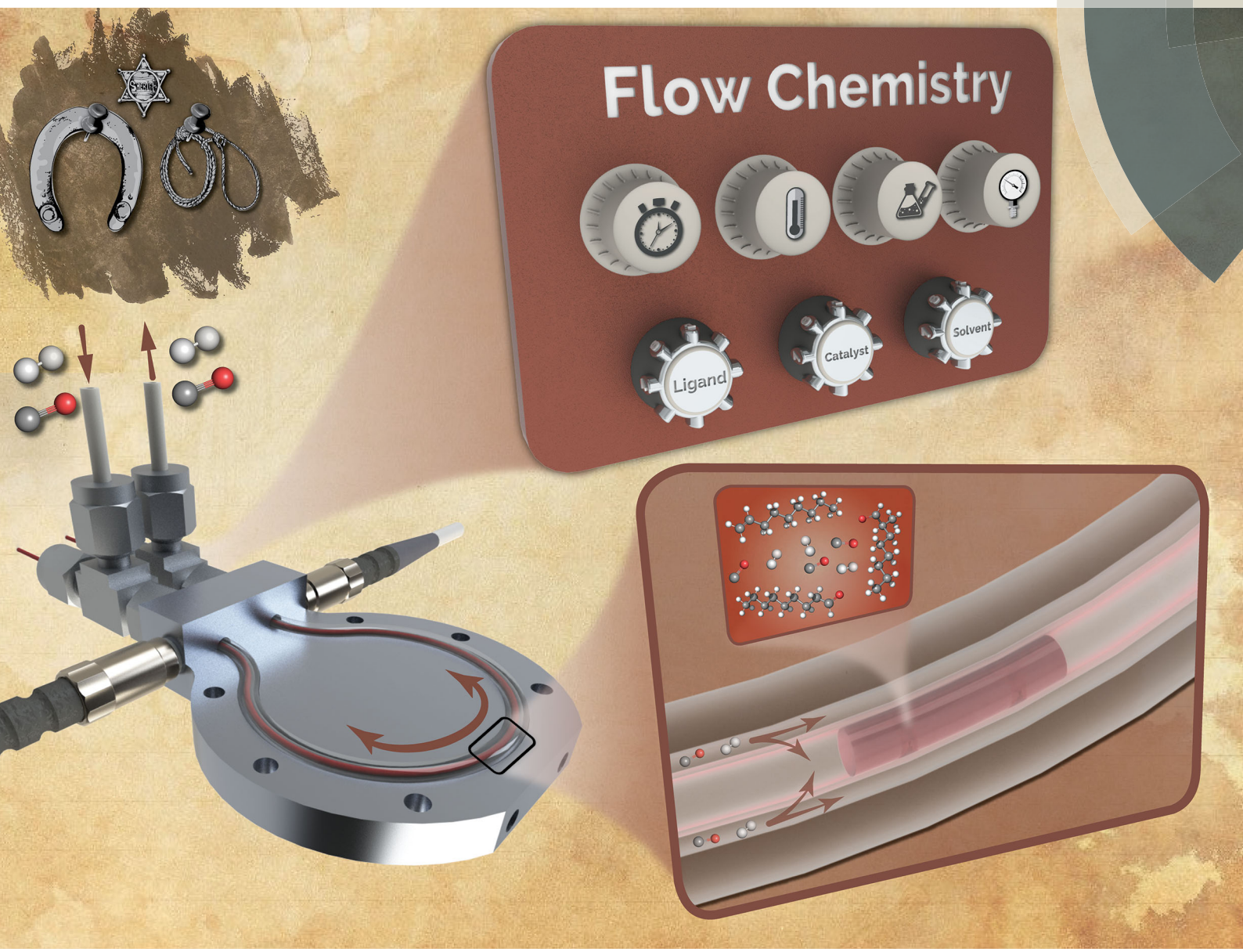

ISSN 1359-7345

ROYAL SOCIETY OF CHEMISTRY

COMMUNICATION

Milad Abolhasani *et al.*

Flow chemistry-enabled studies of rhodium-catalyzed hydroformylation reactions

ChemComm

COMMUNICATION

View Article Online
View Journal | View Issue

Published on 03 July 2018. Downloaded by North Carolina State University on 8/28/2018 4:32:28 PM.

Check for updates

Cite this: *Chem. Commun.*, 2018, **54**, 8567

Received 12th June 2018,
Accepted 3rd July 2018

DOI: 10.1039/c8cc04650f

rsc.li/chemcomm

Flow chemistry-enabled studies of rhodium-catalyzed hydroformylation reactions†

Cheng Zhu,[a] Keshav Raghuvanshi,[a] Connor W. Coley,[b] Dawn Mason,[c] Jody Rodgers,[c] Mesfin E. Janka[c] and Milad Abolhasani *[a]

We present an automated microscale flow chemistry platform for rapid performance evaluation of continuous and discrete reaction parameters in homogeneous hydroformylation reactions. We demonstrate the versatility of the developed microfluidic platform through a systematic study of the effects of a library of phosphine-based ligands on catalytic activity and regioselectivity.

Hydroformylation of alkenes is an important industrial process for production of aldehydes which can be easily converted into many secondary products such as alcohols, plasticizers, and detergents.[1] Today, hydroformylation has become one of the most successful large-scale applications of homogeneous catalysis, where ligands play a significant role in tailoring the properties of conventional cobalt or rhodium (Rh) catalysts.[1a,2] The specially designed ligands can help achieve high catalytic activity, chemoselectivity to aldehydes, and regioselectivity to linear or branched products. Over the past 3 decades, a library of ligands including phosphine or phosphite-based compounds have been developed for regioselective aldehyde production.[1b,c,3]

The hydroformylation process is typically carried out at high pressures (5–30 bar) of carbon monoxide (CO) and hydrogen (H_2) with a temperature range of 40–140 °C.[1–4] The conventional batch reactors utilized for exploratory studies of hydroformylation reactions (*e.g.*, autoclave) suffer from major limitations including large amounts of expensive (*e.g.*, catalyst and ligands) and toxic (*i.e.*, CO) reagents per reaction condition, relatively long reactor start-up and shut-down time delays, and poor heat and mass transfer rates.[4b,5] Recently, flow chemistry has emerged as an efficient technique for fundamental and applied studies of chemical processes operating at high pressure/temperature conditions.[5,6] Microreactor systems are characterized by high surface to volume ratios, enhanced heat and mass transfer rates, and improved accessible parameter space.[5,6] These advantages enable process intensification and precise process control.[5,6b,7] The small internal volume of the microreactor and the reduced sample volume greatly enhance the safety of the reaction and make it an ideal candidate for chemical synthesis processes.[6b]

In this work, we designed and developed an autonomous microscale flow chemistry platform for fundamental and exploratory studies of Rh-catalyzed hydroformylation reactions (Fig. 1 and ESI,† S1). The experimental setup shown in Fig. 1 includes a robotic ligand/catalyst selection module, an injection module, a novel single-droplet microreactor, and an in-line analytical characterization unit. The robotic ligand/catalyst selection module enables on-demand preparation of a single or a mixture of catalysts and ligands (Fig. S1, ESI†), loaded in a vial rack installed within an isolation glovebox (Fig. S5, ESI†) under a positive pressure of nitrogen (N_2) for long term storage and testing of air-sensitive ligands. Using a computer-controlled syringe pump (*cf.* syringe 1 in Fig. 1), a desired amount of selected catalyst/ligand solution(s) is mixed inside the liquid handler

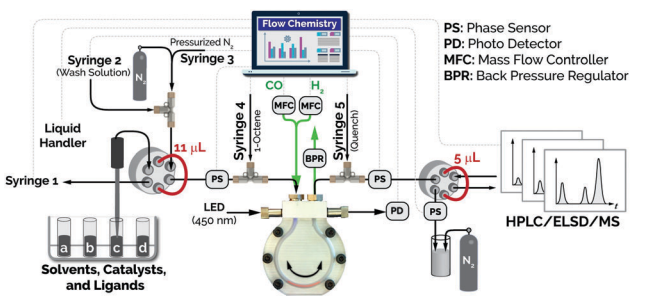

Fig. 1 Schematic of the automated flow chemistry platform developed for fundamental and applied studies of homogeneous hydroformylation reactions. Dashed lines indicate communication with the computer, solid black lines correspond to the fluoropolymer tubing.

[a] *Department of Chemical and Biomolecular Engineering, North Carolina State University, 911 Partners Way, Raleigh, NC 27695, USA. E-mail: abolhasani@ncsu.edu*
[b] *Department of Chemical Engineering, Massachusetts Institute of Technology, 77 Massachusetts Avenue, Cambridge, MA 02139, USA*
[c] *Eastman Chemical Company, 200 S. Wilcox Dr., Kingsport, TN 37660, USA*

† Electronic supplementary information (ESI) available: Automated microfluidic platform design, experimental methods, hydroformylation results, and NMR characterization of ligands. See DOI: 10.1039/c8cc04650f

Published on 03 July 2018. Downloaded by North Carolina State University on 8/28/2018 4:32:28 PM.

needle and injected into a 11 μL sample loop. The droplet is then transferred into the main system flow path (*cf.* solid black lines in Fig. 1), consisting of fluoroethylene propylene (FEP) tubing filled with pressurized N_2 (5–30 bar). A computer-controlled syringe pump (*cf.* syringe 3 in Fig. 1) moves the droplet toward the on-line substrate injection port. A predefined amount of the substrate (1-octene) is then automatically injected into the droplet containing the mixture of catalyst, ligand(s), and solvent using another computer-controlled syringe pump (*cf.* syringe 4 in Fig. 1) before entering the tubular microreactor.

In order to efficiently carry out gas–liquid hydroformylation reactions, a tube-in-tube microreactor configuration (Fig. S2, ESI†) is utilized, wherein a liquid droplet containing the reaction mixture is oscillated back-and-forth through the inner Teflon tubing (Teflon AF 2400) using pressurized nitrogen. Concurrently, a CO/H_2 gas mixture is injected through the annulus between the inner (Teflon AF 2400) and outer (fluorinated ethylene propylene, FEP) tubing, at a defined total pressure and syngas composition, shown in Fig. S2 (ESI†). The syngas ratio is varied using two individually controlled mass flow controllers, while the total syngas pressure is tuned with an adjustable back pressure regulator (Fig. S3, ESI†).

The oscillatory tube-in-tube microreactor is designed to specifically address heat and mass transfer limitations associated with two-phase gas–liquid reactions.[6a,8] The oscillatory motion of the single liquid droplet effectively decouples the interdependency of the average flow velocity and residence time (*i.e.*, reaction time),[9] and provides tunable reaction time ranging between 10 s–1 day within a small reactor volume (66 μL) without sacrificing mixing and mass transfer characteristics (see Movie M1, ESI†).

The high permeability of the inner Teflon tubing for CO and H_2 in comparison with N_2,[6a,10] in combination with the high partial pressure gradient of syngas across the inner tube wall, results in facile permeation of the syngas mixture through the inner tubing (*i.e.*, Teflon AF2400). Furthermore, the oscillatory motion of the liquid droplet provides constant stirring within the reaction mixture (through two recirculation zones inside the liquid slug),[9a,11] thus enhancing the interphase mass transfer. The horseshoe-shaped microreactor design enables single-point optical detection of the liquid droplet at either ends of the Teflon reactor for the automated flow reversal over the course of the hydroformylation reaction. After the desired reaction time, the droplet exits the reactor and is quenched (*cf.* syringe 5 in Fig. 1). Next, using a 5 μL sample loop, an aliquot of the quenched reaction mixture droplet is automatically injected into a high-performance liquid chromatography (HPLC) unit coupled to an evaporative light scattering detector (ELSD) and mass spectrometry (MS) modules for analysis (Fig. S6, ESI†). The remainder of the droplet empties into a pressurized waste vessel (Fig. S4, ESI†).

Utilizing the developed microscale flow chemistry platform, we systematically studied the effect of phosphine-based ligands on Rh-catalyzed hydroformylation of 1-octene (Scheme 1). Computer-controlled preparation of the reaction mixture and operation of the hydroformylation reaction enables precise control of both

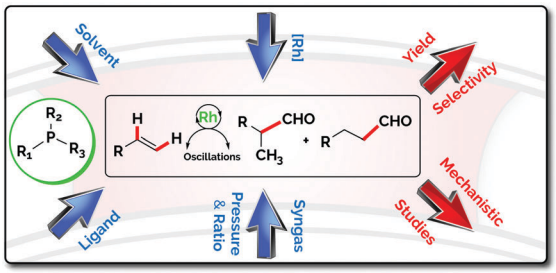

Scheme 1 Hydroformylation of 1-octene using Rh catalyst and phosphine ligands. Blue arrows: experimental input parameter space; red arrows: synthetic outcomes.

continuous (*e.g.*, reaction time, t_R, temperature, T, ligand to catalyst ratio, R_{LC}, syngas pressure, P, and syngas composition, $R_G = H_2:CO$) and discrete (*e.g.*, chemical structure of the ligand and solvent) reaction parameters. The main hydroformylation products are nonanal (linear product, L) and branched aldehydes (B) along with octene isomers from isomerization of the substrate (1-octene) as a side product. The linear and branched aldehydes as well as 1-octene and its isomers were successfully separated by HPLC and confirmed by ELSD and MS (Fig. S6, ESI†).

In the first set of experiments, we studied the operation envelope of 1-octene hydroformylation using the active Rh catalyst, $[RhH(CO)(PPh_3)_3]$, with excess triphenylphosphine, PPh_3, ligand. Fig. 2A shows the HPLC chromatogram evolution of the linear (green curves) and branched (blue curves) products at different reaction times, t_R. Fig. 2B shows the time-evolution of 1-octene conversion over the course of the hydroformylation reaction. The conversion reaches a plateau (90%) after 20 min. Similar conversions of 1-octene were reported previously with a

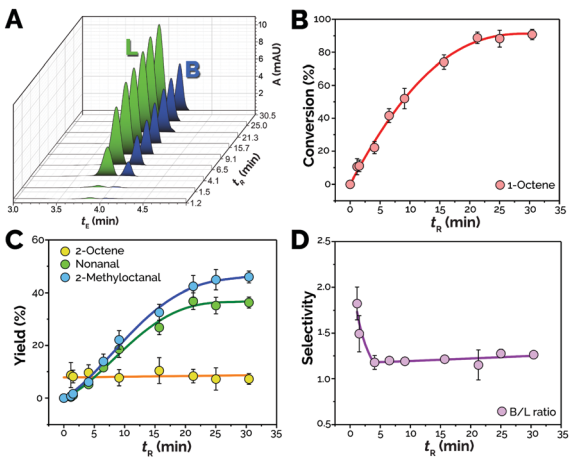

Fig. 2 (A) Time evolution of HPLC chromatograms of aldehyde isomers obtained at different reaction times. Kinetic study of hydroformylation reaction in the flow chemistry setup over 30 min reaction time: (B) 1-octene conversion, (C) 1-octene isomerization and aldehyde yield, and (D) aldehyde regioselectivity (branched : linear). General reaction conditions: 1-octene concentration: 0.5 M, $RhH(CO)(PPh_3)_3$ concentration: 5×10^{-4} M, PPh_3/Rh ratio: 7 : 1, syngas pressure (1 : 1): 6 bar, syngas flow rate: 0.9 mL min^{-1}, carrier nitrogen pressure: 6.5 bar, droplet oscillation flow rate: 100 μL min^{-1}, and T = 90 °C.

 This journal is © The Royal Society of Chemistry 2018

Published on 03 July 2018. Downloaded by North Carolina State University on 8/28/2018 4:32:28 PM.

microscale segmented flow in a silicon microreactor.[5] Similar trends were observed for both linear and branched aldehyde products during the hydroformylation reaction (Fig. 2C), with maximum yields of 36% and 44%, respectively. As shown in Fig. 2C, the initial rate of 1-octene isomerization pathway is significantly faster than aldehyde formation pathways. In addition, 1-octene isomerization doesn't show significant variation over the course of the 30 min hydroformylation reaction. Fig. 2D shows that the regioselectivity of the branched aldehyde initially decreases and reaches a plateau (1.2) after 4 min.

The generally accepted mechanism of monophosphine-Rh(I)-catalyzed hydroformylation was first proposed by Wilkinson *et al.*[12] The most important intermediates in the mechanism are five-coordinate bis(phosphine)rhodium complexes, although complexes with one or three phosphine ligands may also be involved. In the trigonal bipyramidal bis(phosphine)rhodium species, two phosphine ligands occupy either two equatorial sites or one equatorial and one apical site. The aldehyde regioselectivity during hydroformylation reaction is mainly controlled by the tendency of the metal catalyst to attach to the terminal or internal carbon of 1-octene,[1b,5] which is influenced by the coordination of phosphine ligands. When the alkene coordinates with Rh at the internal carbon, it tends to undergo β-elimination to produce isomeric 2-octene.[1b,13] The initial screening experiments (Fig. 2) provided information regarding the conversion and kinetics of 1-octene hydroformylation and validated the developed flow chemistry setup for further mechanistic studies.

In the next step, we utilized the microscale flow chemistry setup to investigate the effect of continuous experimental parameters including reaction temperature, ligand to catalyst ratio, and syngas pressure/composition on the aldehyde yield and regioselectivity using [$Rh(CO)_2(acac)$] as the catalyst and PPh_3 as an exemplary ligand (Fig. 3). Based on our initial hydroformylation results (Fig. 2), the next screening tests were conducted at 20 min reaction time to obtain maximum conversion and chemoselectivity. Fig. 3A shows the effect of reaction temperature on hydroformylation of 1-octene. Higher chemoselectivity to aldehydes was observed with increasing reaction temperature from 60 °C to 100 °C. Increasing the hydroformylation temperature also resulted in an increased isomerization of 1-octene (Fig. S9A, ESI†). A similar behavior is previously reported,[1b,c,5] which can be attributed to higher catalytic activity of bis(phosphine)rhodium complexes at higher temperatures.[1c] At higher reaction temperatures, the catalyst activity is enhanced and results in an increase in the substrate conversion (Fig. S9A, ESI†). Fig. 3B shows that increasing the ligand to catalyst ratio increases the total aldehyde yield, while decreasing the regioselectivity toward the branched aldehyde. A similar trend was observed in the hydroformylation of 1-dodecene with higher linear aldehyde produced at higher ligand to catalyst ratios.[1c] The excess of ligand affects the coordination equilibrium of the rhodium complex,[1c,4b] and suppresses the isomerization of 1-octene.[4b] As indicated in Fig. S9B (ESI†), alkene isomerization yield declined at higher ligand loading. Varying the syngas composition (Fig. 3C) revealed that the addition of H_2 to the

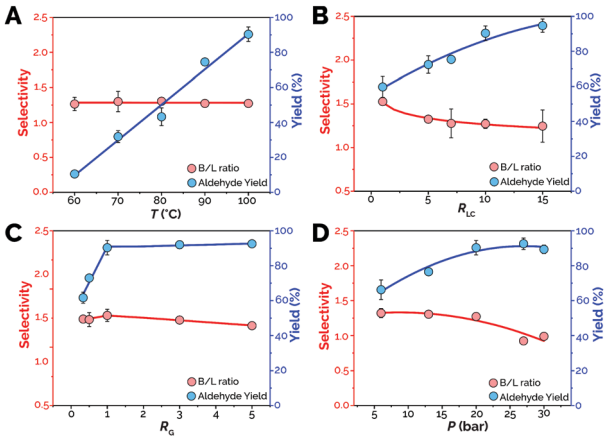

Fig. 3 Effect of (A) temperature, (B) ligand to catalyst ratio, (C) syngas ratio (H_2/CO), and (D) syngas pressure on the aldehyde yield and regioselectivity toward branched isomer obtained using the autonomous flow chemistry platform shown in Fig. 1. General reaction conditions: 1-octene concentration: 0.5 M, $Rh(CO)_2(acac)$ concentration: 5×10^{-4} M, PPh_3/Rh ratio: 10 : 1, syngas pressure (1 : 1): 20 bar, syngas flow rate: 0.3 mL min^{-1}, carrier nitrogen pressure: 20.5 bar, droplet oscillation flow rate: 100 μL min^{-1}, T = 100 °C, and reaction time: 20 min.

rhodium acyl complex is the rate-determining step and the reaction rate is first order with respect to H_2 partial pressure, while the CO has an inhibitory effect in the homogeneous hydroformylation reaction.[5,14] As shown in Fig. 3C and Fig. S9C (ESI†), increasing H_2 : CO ratio increased 1-octene conversion to aldehydes, which is in agreement with a reported mechanistic model.[5] Higher H_2 partial pressure accelerates the cleavage step of aldehyde products from the rhodium complex. However, no significant change was observed in the selectivity toward the branched isomer at different syngas ratios (Fig. 3C). Fig. 3D and Fig. S9D (ESI†) show the effect of syngas pressure on hydroformylation of 1-octene. As shown in Fig. 3D, increasing syngas pressure enhances chemoselectivity toward aldehydes, while decreasing regioselectivity to branched product. The lower dissociation rate of CO from the metal center at high syngas pressures[15] delivers high catalyst activity but with low regioselectivity (branched : linear). These screening tests provide rapid optimization of the experimental parameters which can be utilized in a continuous tube-in-tube reactor for scaled-up hydroformylation reactions.[6a]

In the next set of experiments, we utilized the developed flow chemistry platform to investigate the effect of discrete experimental parameters (*i.e.*, ligand chemical structure) on hydroformylation of 1-octene. We selected a library of traditional phosphine-based ligands and recently emerged Buchwald ligands with different steric and electronic properties, shown in Table 1 and Fig. S10 (ESI†). All hydroformylation reactions were conducted under similar reaction conditions (Table 1) with [$Rh(CO)_2(acac)$] as the catalyst. The selectivity of the produced aldehyde through hydroformylation of alkenes may be governed by the electronic-donating ability of the phosphine ligand. Although the debate continues as to which orbitals on the ligand receives the back-donated electron density, the

Published on 03 July 2018. Downloaded by North Carolina State University on 8/28/2018 4:32:28 PM.

Table 1 Screening of different phosphine and Buchwald ligands in Rh-catalyzed hydroformylation of 1-octene[a]

No.	Ligands	Conversion[b] (%)	Isomer[c] (%)	Aldehyde[d] (%)	B/L[e]
1	PPh_3	95	17	78	53 : 47
2	$P(2\text{-}MePh)_3$	79	22	53	69 : 31
3	$P(2\text{-}OMePh)_3$	83	14	72	69 : 31
4	$P(2\text{-}OMePh)(Ph)_2$	90	13	77	58 : 42
5	$P(4\text{-}MePh)_3$	96	10	88	58 : 42
6	$P(4\text{-}OMePh)_3$	90	6	87	57 : 43
7	$P(4\text{-}MePh)(Ph)_2$	96	2	95	59 : 41
8	$P(4\text{-}FPh)_3$	95	6	89	56 : 44
9	$P(4\text{-}CF_3Ph)_3$	92	5	85	60 : 40
10	$P(Cy)_3$	97	16	80	66 : 34
11	$P(Bz)_3$	80	31	44	61 : 39
12	APhos	91	6	81	56 : 44
13	RockPhos	88	29	60	66 : 34
14	XPhos	90	50	36	68 : 32

[a] General reaction conditions: 1-octene concentration: 0.5 M, $Rh(CO)_2(acac)$ concentration: 5×10^{-4} M, PPh_3/Rh ratio: 10 : 1, syngas pressure (1 : 1): 20 bar, syngas flow rate: 0.3 mL min^{-1}, carrier nitrogen pressure: 20.5 bar, droplet oscillation flowrate: 100 μL min^{-1}, temperature: 100 °C, and reaction time: 20 min. Control experiments see Table S1 (ESI). [b] Alkene conversion determined by HPLC analysis with 1,3,5-trimethoxybenzene as an internal standard (Fig. S7 and S8, ESI). [c] 2-Octene yield was calculated as alkene isomer. [d] Total aldehyde yield. [e] Branched to linear aldehyde ratio.

prevailing view is that donation occurs from the metal d-orbitals to the σ*-orbitals of the phosphorus ligand.[16] It should also be noted that pressure can affect the polarity of {M}–H bond, which is important in controlling the direction of alkene addition to the rhodium complex (Fig. 3D). As shown in Table 1, both methyl (–Me) and methoxy (–OMe) substitution of phosphine ligands resulted in better regioselectivity toward the branched aldehyde in contrast with PPh_3 (Table 1, entries 1–7). *ortho*-Site substitution of ligands showed high regioselectivity compared to *para* substitution. Moreover, higher regioselectivity was observed by a symmetric substitution compared to an asymmetric one (Table 1, entries 2–4). By contrast, *para*-substituted ligands showed relatively low selectivity (Table 1, entries 5–9). Interestingly, decoration of phosphine-based ligands at *para*-position dramatically increased chemoselectivity and lowered alkene isomerization, while maintaining high catalytic efficacy (Table 1, entries 5–9). When investigating the electronic properties of the substituents (Table 1, entries 6 and 9), electron-withdrawing group ($–CF_3$) resulted in slightly higher regioselectivity compared to the electron-donating group (–OMe).[6a] Next, the effect of ligand steric properties on the hydroformylation of 1-octene was studied by a systematic comparison of $P(Cy)_3$, $P(Bz)_3$, and Buchwald ligands with PPh_3 (Table 1, entries 10–14). The steric properties of ligands change the regioselectivity toward the branched aldehyde.[1b]

In conclusion, we developed a microscale flow chemistry platform for accelerated discovery, library screening, and optimization of ligands/catalysts in hydroformylation of alkenes. The single-droplet tube-in-tube microreactor provided enhanced heat and mass transfer rates and removed the start-up/shut-down time delay of batch reactors. The developed flow chemistry approach enabled 43 hydroformylation experiments to be conducted continuously using a total reagent volume less than 1 mL. Furthermore, utilizing the autonomous flow chemistry platform we systematically investigated the catalytic activity, chemoselectivity, and regioselectivity of a library of phosphine-based and Buchwald ligands, illustrating the unique features of *ortho*/*para*-site substituent decorated mono-phosphine ligands.

We thank Eastman Chemical Company for funding this research.

Conflicts of interest

There are no conflicts to declare.

Notes and references

1 (*a*) P. Govender, S. Ngubane, B. Therrien and G. S. Smith, *J. Organomet. Chem.*, 2017, **848**, 281–287; (*b*) A. A. Dabbawala, R. V. Jasra and H. C. Bajaj, *Catal. Commun.*, 2011, **12**, 403–407; (*c*) M. Haumann, H. Koch, P. Hugo and R. Schomäcker, *Appl. Catal., A*, 2002, **225**, 239–249; (*d*) J. October and S. F. Mapolie, *J. Organomet. Chem.*, 2017, **840**, 1–10.
2 C. Li, K. Sun, W. Wang, L. Yan, X. Sun, Y. Wang, K. Xiong, Z. Zhan, Z. Jiang and Y. Ding, *J. Catal.*, 2017, **353**, 123–132.
3 M. Gerlach, D. Abdul Wajid, L. Hilfert, F. T. Edelmann, A. Seidel-Morgenstern, C. Hamel, A. Seidel-Morgenstern, C. Hamel and A. Börner, *Catal. Sci. Technol.*, 2017, **14**, 3832.
4 (*a*) M. Dessoudeix, M. Urrutigoity and P. Kalck, *Eur. J. Inorg. Chem.*, 2001, 1797–1800; (*b*) E. Vunain, P. Ncube, K. Jalama and R. Meijboom, *J. Porous Mater.*, 2017, 1–18.
5 J. Keybl and K. F. Jensen, *Ind. Eng. Chem. Res.*, 2011, **50**, 11013–11022.
6 (*a*) S. Kasinathan, S. L. Bourne, P. Tolstoy, P. Koos, M. Obrien, R. W. Bates, I. R. Baxendale and S. V. Ley, *Synlett*, 2011, 2648–2651; (*b*) J. Yue, J. C. Schouten and T. A. Nijhuis, *Ind. Eng. Chem. Res.*, 2012, **51**, 14583–14609; (*c*) T. Noël and S. L. Buchwald, *Chem. Soc. Rev.*, 2011, **40**, 5010–5029; (*d*) T. Noel, S. Kuhn, A. J. Musacchio, K. F. Jensen and S. L. Buchwald, *Angew. Chem., Int. Ed.*, 2011, **50**, 5943–5946; (*e*) S. Marre, A. Adamo, S. Basak, C. Aymonier and K. F. Jensen, *Ind. Eng. Chem. Res.*, 2010, **49**, 11310–11320; (*f*) X. Wang, *J. Flow Chem.*, 2015, **5**, 125–132.
7 V. Hessel, D. Kralisch, N. Kockmann, T. Noël and Q. Wang, *ChemSusChem*, 2013, **6**, 746–789.
8 (*a*) T. Noël and V. Hessel, *ChemSusChem*, 2013, **6**, 405–407; (*b*) F. Reichmann, A. Tollkötter, S. Körner and N. Kockmann, *Chem. Eng. Sci.*, 2017, **169**, 151–163; (*c*) Y.-J. Hwang, C. W. Coley, M. Abolhasani, A. L. Marzinzik, G. Koch, C. Spanka, H. Lehmann and K. F. Jensen, *Chem. Commun.*, 2017, **53**, 1–4; (*d*) S. K. Yap, Y. Yuan, L. Zheng, W. K. Wong, J. Zhang, N. Yan and S. A. Khan, *Green Chem.*, 2014, **16**, 4654–4658.
9 (*a*) M. Abolhasani, C. W. Coley and K. F. Jensen, *Anal. Chem.*, 2015, **87**, 11130–11136; (*b*) M. Abolhasani, N. C. Bruno and K. F. Jensen, *Chem. Commun.*, 2015, **51**, 8916–8919; (*c*) C. W. Coley, M. Abolhasani, H. Lin and K. F. Jensen, *Angew. Chem., Int. Ed.*, 2017, **56**, 9847–9850.
10 P. B. Cranwell, M. O'Brien, D. L. Browne, P. Koos, A. Polyzos, M. Peña-López and S. V. Ley, *Org. Biomol. Chem.*, 2012, **10**, 5774.
11 M. Abolhasani, A. Oskooei, A. Klinkova, E. Kumacheva and A. Günther, *Lab Chip*, 2014, **14**, 2309–2318.
12 D. Evans, J. A. Osborn and G. Wilkinson, *J. Chem. Soc. A*, 1968, 3133–3142.
13 R. Lazzaroni, P. Pertici, S. Bertozzi and G. Fabrizi, *J. Mol. Catal.*, 1990, **58**, 75–85.
14 R. M. Deshpande, H. Delmas and R. V. Chaudhari, *Ind. Eng. Chem. Res.*, 1996, **35**, 3927–3933.
15 L. H. Slaugh and R. D. Mullineaux, *J. Organomet. Chem.*, 1968, **13**, 469–477.
16 (*a*) W. Strohmeier and F.-J. Müller, *Eur. J. Inorg. Chem.*, 1967, 2812–2821; (*b*) S. X. Xiao, W. C. Trogler, D. E. Ellis and Z. Berkovitch-Yellin, *J. Am. Chem. Soc.*, 1983, **105**, 7033–7037; (*c*) W. A. Henderson and C. A. Streuli, *J. Am. Chem. Soc.*, 1960, **82**, 5791–5794; (*d*) C. A. Streuli, *Anal. Chem.*, 1960, **32**, 985–987; (*e*) C. A. Tolman, *Chem. Rev.*, 1977, **77**, 313–348; (*f*) T. L. Brown and K. J. Lee, *Coord. Chem. Rev.*, 1993, **128**, 89–116; (*g*) T. L. Brown, *Inorg. Chem.*, 1992, **31**, 1286–1294.

 This journal is © The Royal Society of Chemistry 2018